Proceedings of the ASME 2019 14th International Manufacturing Science and Engineering Conference
MSEC2019
June 10-14, 2019, Erie, PA, USA

MSEC2019-2848

UNDERSTANDING THE LASER-MATTER INTERACTION AND PLASMA DYNAMICS IN NANOSECOND PULSED LASER SHOCK PROCESSING: A FIRST PRINCIPLE STUDY

Bo Mao and Yiliang Liao*

Department of Mechanical Engineering, University of Nevada, Reno, Reno, NV 89557
Corresponding author email:yliao@unr.edu

ABSTRACT

Laser-matter interaction and plasma dynamic during laser shock processing determine the key parameters such as laser shock wave pressure and evolution during laser shock processing (LSP) process. A first-principle based model is critically important for elucidating the underlying mechanism and process optimization of the LSP process. The current study focuses on developing a theoretical model for the fundamental understanding of laser-matter interaction and plasma dynamics. The key physical parameters, such as electron and ion temperature, plasma density and shockwave pressure are predicted by this model and validated by experimental results.

Keywords: Laser Shock Processing; Modeling; Laser-matter Interaction; Plasma Dynamics; Shockwave Pressure.

NOMENCLATURE

T_e = electron temperature
T_i = ion temperature
C_e = heat capacities (per unit volume) for electrons
C_i = heat capacities (per unit volume) for ions
p_e = energy density for electrons
p_i = energy density for ions
q = Von-Neumann artificial viscosity
V = specific volume
κ_e= thermal conductivity for electrons
κ_i= thermal conductivity for ions
k_B = Boltzmann constant
m_e = electron mass
e = electron charge
Λ_{ei}= Coulomb terms for electron-ion collisions
Λ_{ii}= Coulomb terms for ion-ion collisions
Z = mean charge of the plasma
E_e= specific internal energies for electrons
E_i= specific internal energies for ions
σ_g^{PA}= Planck mean opacities for absorption
σ_g^{PE}= Planck mean opacities for emission
$I(t)$ = Laser intensity as a function of time
R= Reflectivity of the ablative materials
α= absorption coefficient of the ablative materials
μ = magnetic permeability
σ_0= electrical conductivity
f= the frequency of the electromagnetic wave
τ_e=electrons relaxation time
τ_i=ions relaxation time
τ_L=duration time
g= frequency group index
N_F =number of frequency groups
c =the speed of light
w= angular frequency,
k = Boltzmann's constant
z= depth of investigated point
P_e=plasma pressure due to electrons
P_i= plasma pressure due to ions
P_r= plasma pressure due to radiations
q = von Neumann artificial viscosity
N_A = Avogadro's number,
A = the ion atomic weight
S_v= the scattering coefficient.
σ_{SB}= Stefan-Boltzmann constant
σ_P^E= Planck emission opacity
$B_v(T)$= Planck function at temperature T
U = shockwave propagation speed
u = expansion speed of particles

INTRODUCTION

Laser-based advanced manufacturing process has been extensively studied and developed in recent years. Among a variety of laser-based materials processing techniques, nanosecond laser shock processing (LSP) has gained tremendous research interests due to its high flexibility, desirable controllability, and broad applicability [1, 2]. During LSP process, the laser-induced shock wave with a high peak pressure (in an order of GPa) and ultra-short duration time (in an order of

nanoseconds) is utilized to process materials [3]. Typical examples of LSP include laser shock peening [4], laser surface patterning [5], laser peen forming [6], and laser shock imprinting [7].

A schematic illustration of the LSP process is shown in Figure 1. An ablative coating layer is put on the top of the target surface for absorbing the laser energy and protecting the sample. A transparent confinement is placed on the top of the ablative coating. Once the ablative coating is irradiated by the laser energy, it is evaporated and ionized immediately, resulting in a laser-induced plasma with high density and high temperature. Since dynamic expansion of the plasma is confined by the confinement, laser shockwave with high peak pressure is generated and propagates into the target material [8, 9]. Therefore, ultra-high strain rate deformation and compressive residual stress is induced in the near surface layer, which can be utilized to improving the surface strength [10] , fatigue endurance [11] , stress corrosion resistance [12] of the processed materials.

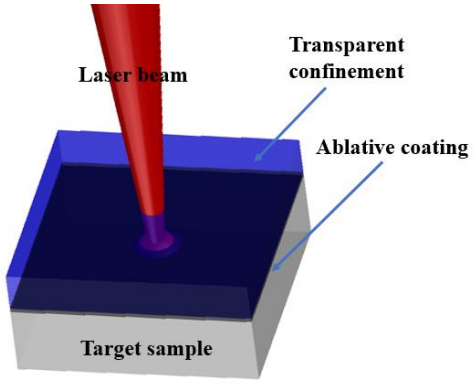

Figure 1: Schematic illustration of LSP process.

Despite extensive research efforts have been paid in LSP study, most of them focus on their process development and optimization [4, 13-17]. During LSP process, the key beneficial characteristics is the shockwave which resulted from the laser-matter interactions. The plasma dynamics during LSP process determines the magnitude, temporal and spatial evolution of the shockwave pressure. Therefore, physics-based modeling of laser-matter interactions and plasma dynamics during LSP process is of significant importance. The most widely used LSP model is proposed by Fabbro et al [18] and further developed by Zhang et al. [19]. However, these physical mechanism in these models are highly simplified. Some advanced physics-based models were proposed by other researchers [18, 20-27] in recent years. However, the spatial and temporal evolution of plasma state variables were not systematically studied, resulting in their limited applications.

The current paper aims at understanding the laser-matter interaction and plasma dynamic during LSP process based on first principle study. A physics-based model is proposed by considering both the laser energy absorption and plasma formation. The electron and plasma state variables, as well as the propagation of laser shockwave is predicted by the model. The modeling results are validated by experimental data and show good agreement.

MODEL DESCRIPTION

In our model, particular focus will be put on the laser absorption and resultant laser-induced plasma dynamic process. Therefore, the entire LSP process is divided into two stages. Stage one is absorption and conduction of the laser pulse, and stage two involves the formation and expansion of the laser-induced plasma. All the physical phenomenon in our model will be studied based on first-principle physics.

Stage 1: Absorption and conduction of laser energy

During LSP process, once the laser pulse transmits through the transparent confinement and interacts with the ablative coating, the laser energy is rapidly absorbed by the electrons near the Femi surface. This process typically finishes in femtoseconds. Afterwards, the electrons with high temperature starts to interact with the neighboring lattice via electron-photon emission, resulting in the thermal equilibrium between electron and lattice within in tens of picoseconds. The thermodynamic process of electrons and lattices can be described by the well-known two temperature mode [28, 29]:

$$C_e \frac{\partial T_e}{\partial t} = \nabla\bullet(k_e \nabla T_e) - \Gamma_{ei}(T_e - T_i) - (\frac{\partial E_e}{\partial V} + p_e)\frac{\partial V}{\partial t} + R_{Abs} - R_{Emis} + S \quad (1)$$

$$C_i \frac{\partial T_i}{\partial t} = \nabla\bullet(k_i \nabla T_i) + \Gamma_{ei}(T_e - T_i) - (\frac{\partial E_i}{\partial V} + p_i)\frac{\partial V}{\partial t} - q\frac{\partial V}{\partial t}$$

The thermal conductivities for electrons and irons κ_e and κ_i are given by:

$$k_{e,i} = 20(\frac{2}{\pi})^{3/2} \frac{(k_B T_{e,i})^{5/2} k_B \tau_{e,i}}{m_e^{1/2} e^4 Z \ln \Lambda_{ei,ii}} \quad (2)$$

$\tau_i = 1$ and $\tau_e = 0.43Z/(3.44 + Z + 0.26\,ln\,Z)$. The electron-phonon coupling constants are giving by: $\Gamma_{ei} = C_e \frac{Z^2 \ln \Lambda_{ei}}{A^2 V T_e^{3/2}}$. Moreover, the radiation absorption and emission terms R_{Abs} and R_{Emis} can be expressed by [29]:

$$R_{Emis} = \frac{8\pi(k_B T_e)^4}{c^3 h^3} \sum_g^{N_F} (\sigma_g^{PE} \int_{x_g}^{x_{g+1}} \frac{x^3}{e^x - 1} dx), \quad x = \frac{\hbar\omega}{k_B T_e}, \quad (3)$$

$$R_{Abs} = c \sum_g^{N_f} (\sigma_g^{PA} E_{R,g}), \quad (4)$$

The incident laser energy is the source term in equation 1 and can be expressed by [30]:

$$S = \alpha(1-R)I(t)\left(\frac{w_0}{w}\right)^2 e^{-2r^2/w^2} e^{-\alpha z} \quad (5)$$

The absorption coefficient, α, is determined by the skin-depth δ of electromagnetic wave penetrating into the metal, $\alpha = 1/\delta,\ \delta = 1/\sqrt{\pi\mu f\sigma_0}$, Since for the nanosecond pulse laser, $\tau_e \ll \tau_i \ll \tau_L$ is fulfilled, therefore it can be assumed that the electrons and ions can reach thermodynamic equilibrium very quick.

In our work, the Bremsstrahlung model is used for describing the evolution of electron and ion density. Therefore, for a given laser with a wavelength of λ_L, the critical density of electrons and ions can be estimated by [31]:

$$\begin{aligned} n_{e,crit} &= \frac{\varepsilon_0 m_e}{e^2}, \\ \omega_L^2 &= (1.11\times10^{21} cm^{-3})\lambda_{L,\mu m}^{-2} \end{aligned} \quad (6)$$

The depth at which the laser light penetrates (in which below the laser is unable to penetrate) can be deduced from the absorption coefficient [32]:

$$\kappa = (2\pi)^{1/2}\left(\frac{16\pi}{3}\right)\frac{e^6}{c(m_e k T_e)^{3/2}} Z\, n_e^2 \frac{\ln\Lambda}{\omega_L^2\sqrt{1-(\omega_P/\omega_L)^2}}, \quad (7)$$

where k is Boltzmann's constant, n_e is the electron density, T_e is the electron temperature, Z is the mean charge of the plasma, and the Coulomb logarithm $\ln\Lambda$ is are computed using simple semi-empirical formulas [33] and do not include quantum effects.

Stage 2: laser induced plasma dynamics

During nanosecond LSP process, the mechanism behind the ionization lies in the collision of the fast electrons. Therefore, the net energy gained from collision process can be estimated by [30]:

$$\left(\frac{dE}{dt}\right)_{gain} = \left(\frac{8k_B}{\pi}\right)^{1/2}\frac{ne^2 I}{m^{3/2}\varepsilon_0 c\omega^2}\sigma T_e^{1/2}, \quad (8)$$

where σ is the collision cross section, n is the number density, and ε_0 is the vacuum permeability.

As the plasma is generated during ionization process, the plasma dynamics can be described by the macroscopic two fluid mode. The state variables of plasma can be are obtained by taking the moments on the entire Vlasov equation and assuming the Maxwell-Boltzmann conditions [28]:

$$\frac{\partial f_\sigma}{\partial t} + \frac{\partial f_\sigma}{\partial \vec{x}}\cdot\frac{d\vec{x}}{dt} + \frac{\partial f_\sigma}{\partial \vec{v}}\cdot\frac{d\vec{v}}{dt} = \sum\nolimits_\alpha C_{\sigma\alpha}(f_\sigma), \quad (9)$$

where f(x,v,t) is the plasma function to denote the instantaneous configuration of the plasma. $C_{\sigma\alpha}(f_\sigma)$ is the change rate of the distribution function f_σ due to collisions of species σ with species α.

The continuity equation for each species σ is obtained by integrating Eq.8 over velocity for each species. The "zeroth moment" of Vlasov equation becomes [28, 34]:

$$\frac{\partial n_\sigma}{\partial t} + \nabla\cdot(n_\sigma \overrightarrow{u_\sigma}) = 0, \quad (10)$$

where $n_\sigma = \int f_\sigma dv$ is the number density and $\vec{u}_\sigma = \int v f_\sigma dv / n_\sigma$ is the mean velocity.

In one-dimensional case, mass conversion equation is proposed by [35]:

$$\frac{\partial V}{\partial t} = V\frac{\partial u}{\partial t} = \frac{\partial u}{\partial m_0} \quad (11)$$

As a result, the plasma velocity in electro-magnetic field $\vec{E}$ and $\vec{B}$ can be obtained by calculated by [28, 34]:

$$n_\sigma m_\sigma \frac{\partial \overrightarrow{u_\sigma}}{\partial t} + n_\sigma m_\sigma(\overrightarrow{u_\sigma}\cdot\nabla)\overrightarrow{u_\sigma} = n_\sigma q_\sigma\left(\vec{E} + \overrightarrow{u_\sigma}\times\vec{B}\right) - \nabla P_\sigma - \overrightarrow{R_{\sigma\alpha}}, \quad (12)$$

where $\vec{R}_{\sigma\alpha}$ is the net frictional drag force due to collisions of species σ with species α.

In one-dimensional case, the momentum conservation equation is proposed by [35]:

$$\frac{\partial u}{\partial t} = -\frac{1}{\rho}\frac{\partial}{\partial r}(P+q) = -\frac{\partial}{\partial m_0}(P+q) + \dot{u}_{TN}, \quad (13)$$

where $\dot{u}_{TN}$ is the velocity change due to momentum exchange from the slowing down of fast particles and P is the plasma pressure which can be estimated by the sum of electron pressure, ion pressure, and radiation pressure. By multiplying the Vlasov equation with factor $m_\sigma v^2/2$ and integrating over the N-dimensional velocity space, the second moment can be written as [28, 36]:

$$\begin{aligned} &\frac{N}{2}\frac{\partial P_\sigma}{\partial t} + \frac{N}{2}\vec{u}_\sigma\cdot\nabla P_\sigma + \frac{2+N}{2}P_\sigma\nabla\cdot\vec{u}_\sigma = -\nabla\cdot\vec{Q}_\sigma + \\ &\vec{R}_{\sigma\alpha}\cdot\vec{u}_\sigma - \left(\frac{\partial W}{\partial t}\right)_{E\sigma\alpha} \end{aligned}, \quad (14)$$

where the first term $-\nabla\cdot\vec{Q}_\sigma$ indicates the heat flux, the second term represents the heating of species σ induced by the frictional drag on species α, and the last term $(\partial W/\partial t)_{E\sigma\alpha}$ is the rate of energy transfer from species σ to species α due to collisions. The second moment of the Vlasov equation indicates the energy evolution of the plasma flow.

Parameters and Boundary Conditions

During laser matter interactions, the temperature of ions and electrons are much higher than the Femi temperature, and

therefore, the thermal conductivity and electron-ion coupling coefficients are varied with temperature and can be given by [29, 35]:

$$k_e = 20(\frac{2}{\pi})^{\frac{3}{2}} \frac{(k_B T_e)^{\frac{5}{2}} k_B \varepsilon\delta_T}{e^4 Z\sqrt{m_e}\ln\Lambda_{ei}}$$
$$\varepsilon\delta_T = \frac{0.43Z}{3.44+Z+0.26\ln Z} \quad (15)$$
$$\ln\Lambda_{ei} = \max\{1, \ln\frac{3}{2e^3}\sqrt{\frac{k_B^3 T_e^3}{\pi n_e}}\frac{1}{Z}\}$$

The thermal conductivity of ion is given by:

$$k_i = 20(\frac{2}{\pi})^{3/2} \frac{(k_B T_e)^{5/2} k_B}{e^4 Z\sqrt{m_e}\ln\Lambda_{ii}}$$
$$\ln\Lambda_{ii} = \max\{1, \ln(\frac{3}{2e^3 Z^2})\sqrt{\frac{k_B^3 T_e^3}{\pi n_e}}\frac{1}{\sqrt{Z}}\} \quad (16)$$

The electron-ion coupling coefficient is given by:

$$\Gamma_{ei} = C_{ve}\frac{8\sqrt{2\pi}}{3} N_A^2 e^4\sqrt{m_e}(\frac{Z}{A})^2\frac{\rho\ln\Lambda_{ei}}{(k_B T_e)^{3/2}} \quad (17)$$

Moreover, the permissible flux limit is defined to avoid the unusual thermal fluxes due to the breaking down effect:

$$q_{\max} = \frac{3\sqrt{3}}{8} n_e k_B T_e\sqrt{\frac{k_B T_e}{m_e}} \quad (18)$$

The multi-group diffusion process is considered and can be expressed by [29, 35]:

$$V\frac{\partial E_R^g}{\partial t} = \frac{\partial}{\partial m_0}(k_R^g\frac{\partial E_R^g}{\partial r}) - \frac{4}{3}E_R^g\dot{V} - c\sigma_{P,A}^g E_R^g + J^g \quad , \quad (19)$$

where J is the emission term and can be described as $J = 4\sigma_{SB}V\sigma_P^E T_e^4$. Since the emission occurs in multi-groups during the interaction, the total emission term is written by the summation:

$$J = \sum_{g=1}^{N} J_g$$
$$J_g = \frac{8\pi(k_B T_e)^4}{c^2 h^3}\sigma_{P,g}^E\int_{x_g}^{x_g+1}\frac{x^3}{e^x-1}dx \quad (20)$$
$$x_g = \frac{h\nu_g}{k_B T_e}$$

The absorption term in the multi-frequency group can be estimated by:

$$A = \sum_{g=1}^{N} c\sigma_P^g E_R^g \quad (21)$$

Since the electrons and irons and assumed to reach thermal equilibrium immediately after laser irradiation, which is described as local thermodynamic equilibrium (LET). The atomic level populations are obtained from Boltzmann statistics and the Saha equation. Therefore, the group opacities are given by:

$$\sigma_g^{PA} = \frac{1}{\rho}\frac{\int_{x_g}^{x_g+1} dx\ B_\nu(T)\kappa_\nu}{\int_{x_g}^{x_g+1} dx\ B_\nu(T)}$$
$$\sigma_g^{PE} = \frac{1}{\rho}\frac{\int_{x_g}^{x_g+1} dx\ \eta_\nu}{\int_{x_g}^{x_g+1} dx\ B_\nu(T)} \quad (22)$$
$$\sigma_g^{R} = \frac{1}{\rho}\frac{\int_{x_g}^{x_g+1} dx\ (\frac{\partial B_\nu}{\partial T})}{\int_{x_g}^{x_g+1} dx\ (\frac{\partial B_\nu}{\partial T})\frac{1}{\kappa_\nu+s_\nu}}$$

RESULTS AND DISCUSSION

Figure 2 presents the experimental measurements [20] and simulation results of the peak pressure of laser shockwave during underwater LSP with various laser intensities and a pulse duration of 25 ns. It is found that the peak pressure linearly increases with the increase of laser intensity. For instance, the peak pressure increases from 1.2 to 4.5 GPa as the laser intensity increases from 1 to 8 GW/cm^2. Moreover, it is demonstrated in Figure 2 that the simulation results are relatively accurate, but slightly higher than the experimental measurements. Such discrepancy might be caused by the beam energy loss due to the absorption and reflection by water confinement.

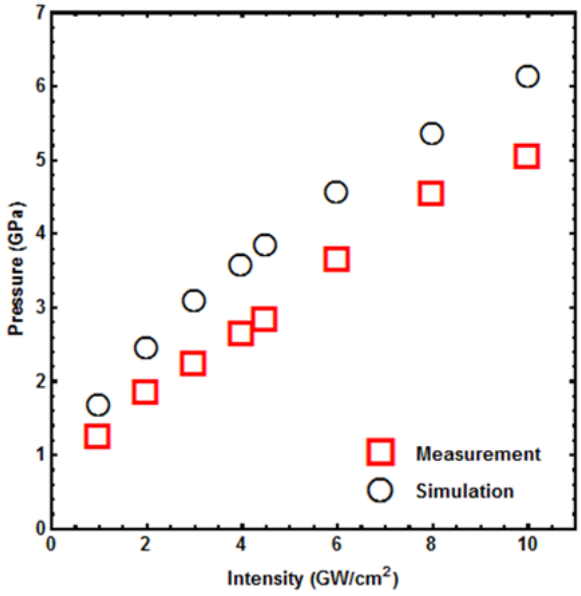

Figure 2: A comparison of the predicted shockwave pressure with experimental results in under water LSP process [20].

Figure 3(a) presents a comparison between simulation results and experimental measurements of the temporal evolution of laser shock pressure during LSP with a laser intensity of 8 GW/cm^2 and a pulse duration of 10ns [22]. It can be found that simulation results are consistent with the trend of the experimental data. Moreover, the laser shockwave pressure rapidly increases to a maximum value of 5 GPa at 6 ns, which can be observed in both simulation and experiment. Later on, the pressure starts to decrease at a slow rate and remains above 1.5 GPa for more than 50 ns, due to the confining effect of water. Figure 3(b) presents the simulated temporal evolution of shockwave pressure during underwater LSP with laser intensities of 2, 5, and 8 GW/cm^2. It is found that the magnitude of peak pressure increases with the increase of laser intensity.

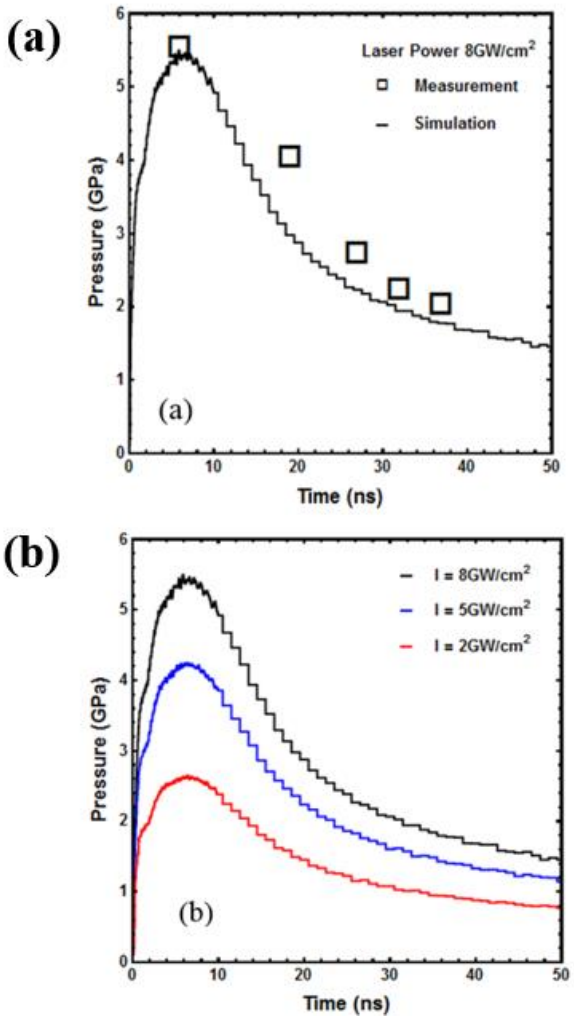

Figure 3: (a) Comparison of the predicted temporal evolution of shockwave pressure with experimental data at a laser intensity of 8.0 GW/cm^2. (b) Comparison under different laser intensities.

Figure 4(a) and (b) show comparisons between the experimental data and model predictions of LSP process with a water confinement and a glass confinement, respectively. It is found that the model predictions are reasonable accurate at low laser intensities ($\leq$3 GW/cm^2), while show large deviations at high laser intensities because the response of equations of state (EOS) would be highly nonlinear at high temperature. In addition, for underwater LSP, the model predictions are found to be higher than the experimental data. This might be attributed to the energy loss due to absorption by water and weak confining effect due to limited thickness of a few millimeters. On the other hand, for LSP with a glass as the confinement, the model predictions are found to be lower than experimental data. This can be explained by the strengthened confining effect at the rigid confinement/ablative coating interface. Figure 4(c) and (d) shows the predicted temporal and spatial evolution of the plasma pressure during LSP with a laser intensity of 5 GW/cm^2 and 8 GW/cm^2 using a glass as the confinement. The vertical axis stands for the position of the sample assembly, i.e., the substrate is located from 0 to 1 cm, the ablative coating from 1 to 1.0005 cm and the glass from 1.0005 to 2.0005 cm. The simulation results show that the peak pressure appears at the top of the ablative coating (1.0005 cm) due to the plasma ignition. A V-shape on the contour plot can be observed, indicating the shock pressure propagates into the adjacent medium. For example, at the instant moment of 30 ns in Figure (c), the pressure penetrates into the substrate at a depth of 0.01 cm.

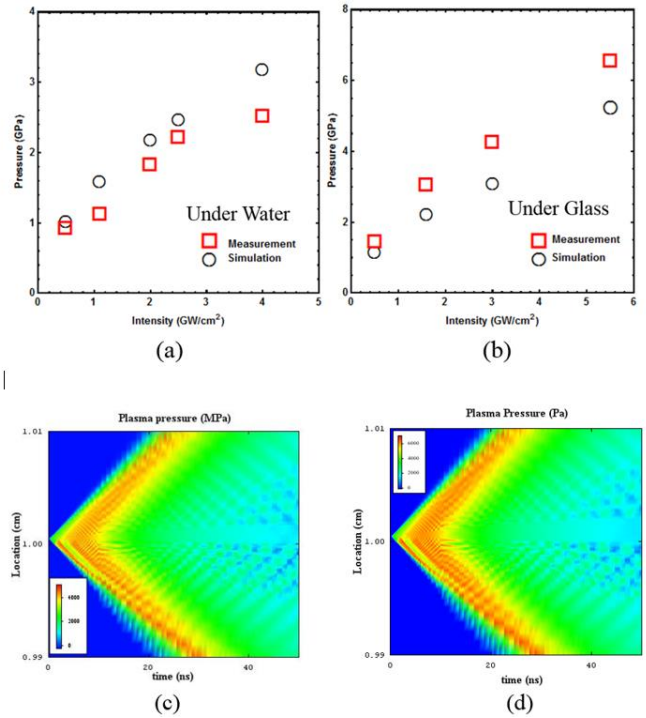

Figure 4: Comparisons of the predicted shockwave peak pressure in LSP process with experimental data from [37]. (a) LSP was performed with water as confinement and (b) LSP was

performed with glass as confinement. The predicted temporal plasma pressure distribution in LSP with a laser intensity of (c) 5 GW/cm^2 and (d) 8 GW/cm^2.

In addition to laser shock pressure, the proposed LSP model is capable of predicting essential parameters including electron temperatures and particle velocities during plasma expansion. Figure 5(a) and (b) present the temporal and spatial evolution of electron temperature during glass-confined LSP with a laser intensity of 5 and 8 GW/cm^2, respectively. As shown in Figure 5(a), the electron temperature reaches to a maximum value of 6 eV at the glass/ablative coating interface, and sustains for ~ 15 ns. Later on, the electron temperature at the interface rapidly decreases to 3 eV in 20 ns. For a fixed time shot, the temperature decreases rapidly as the distance increases from the center, indicating the expansion effect of the plasma. Figure 5(b) shows a similar scenario in the case of LSP with a laser intensity of 8 GW/cm^2. It is found that the maximum electron temperature is increased to 8 eV, and the expansion profile is broader as compared to Figure 5(a). Figure 5(c) presents a comparison between simulation results and experimental data of the temporal evolution of electron temperature as affected by plasma expansion [38]. It is found that the model prediction matches well with the measurements. For example, a decay of electron temperature from 2.7 to 1.4 eV in 80 ns is observed in both simulation and experiment.

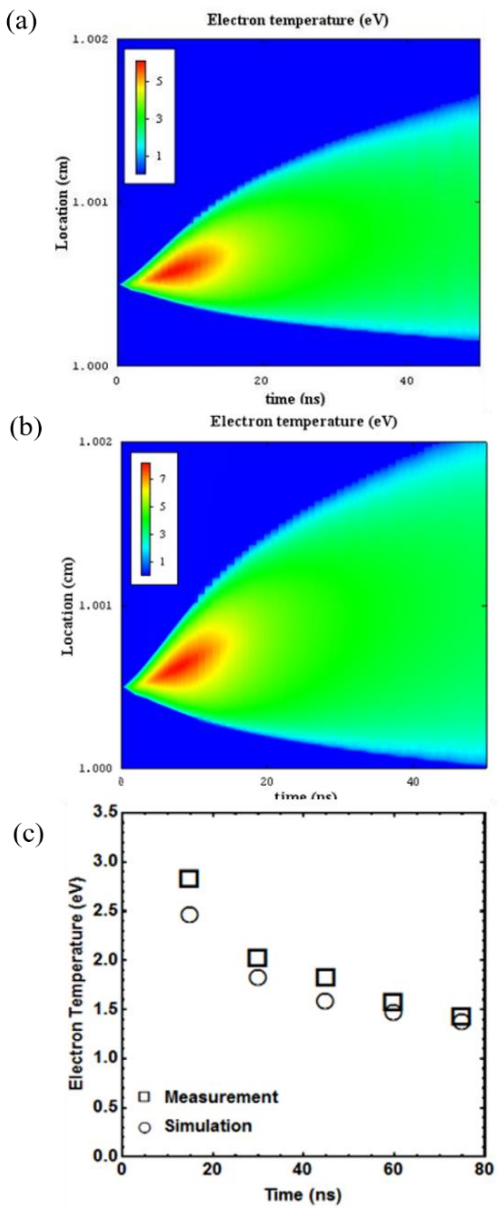

Figure 5: Predicted temporal evolution of temperature distribution of plasma in LSP with laser intensity of (a) 5 GW/cm^2, and (b) 8 GW/cm^2. (c) Comparison of the predicted electron temperature with experimental data from [38].

Figure 6(a) and (b) present the temporal and spatial evolution of the fluid velocity during the plasma expansion in glass-confined LSP with a laser intensity of 5 and 8 GW/cm^2, respectively. The velocity of fluid expansion is marked by red (positive values) and blue (negative values) colors for opposite velocity directions, where the upward direction is defined as positive. It can be observed that the plasma front propagates at a speed of 40000 cm/s, within a band (mark in red color) of width 0.003 cm. The expansion velocity decays rapidly from 40000 to 20000 cm/s in around 10 ns. Comparisons of modeling results

and experimental data on the particle velocities and the shockwave front distance are shown in Figure 6(c), and (d), respectively. As observed in Figure 6(c), given a laser intensity 2 GW/cm^2 and a pulse duration of 25 ns [20], both modeling results and experimental data indicate that the plasma expansion velocity decays from 230 to 50 m/s in 100 ns. Figure 6(d) shows the location of shockwave front as time evolves. Based on Fig.6d, the shockwave speed can be estimated to be around 6 km/s [39]. Since the relationship between particle velocity and plasma velocity can be described as $U=C_0+Su$ [20]. The constants can be deduced by our model: C_0 = 5390 m/s and S = 1.34.

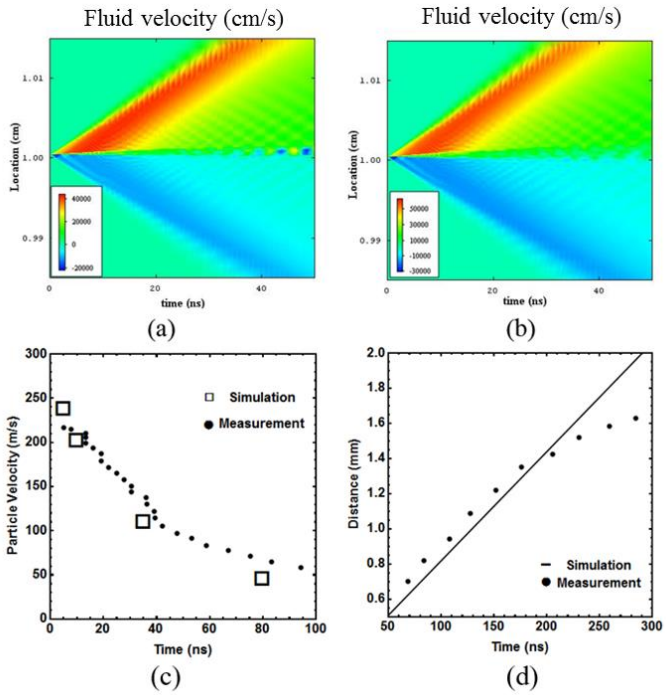

Figure 6: Predicted plasma propagation velocity field in LSP process with a laser intensity of (a) 5 GW/cm^2, and (b) 8 GW/cm^2. Validations of the predicted results with experimental data from [20, 39]: (c) particle velocities and (d) distance the shockwave propagated.

CONCLUSIONS

In this paper, a physical model based on first-principle study is developed to investigate the laser matter interactions and plasma dynamics during LSP process. The key physical parameters, such as electron and ion temperature, plasma density and shockwave pressure are predicted by this model and validated by experimental results. We envision the model in this study will provide guidance and insights for understanding, describing and future design of the laser shock based materials processing and advanced manufacturing.

REFERENCES

[1] Peyre, P., and Fabbro, R., 1995, "Laser shock processing: a review of the physics and applications," Optical and quantum electronics, 27(12), pp. 1213-1229.

[2] Shukla, P. P., Swanson, P. T., and Page, C. J., 2014, "Laser shock peening and mechanical shot peening processes applicable for the surface treatment of technical grade ceramics: a review," Proceedings of the Institution of Mechanical Engineers, Part B: Journal of Engineering Manufacture, 228(5), pp. 639-652.

[3] Montross, C. S., Wei, T., Ye, L., Clark, G., and Mai, Y.-W., 2002, "Laser shock processing and its effects on microstructure and properties of metal alloys: a review," Int. J. Fatigue, 24(10), pp. 1021-1036.

[4] Mao, B., Liao, Y., and Li, B., 2018, "Gradient twinning microstructure generated by laser shock peening in an AZ31B magnesium alloy," Appl. Surf. Sci., 457, pp. 342-351.

[5] Mao, B., Siddaiah, A., Menezes, P. L., and Liao, Y., 2018, "Surface texturing by indirect laser shock surface patterning for manipulated friction coefficient," J. Mater. Process. Technol., 257, pp. 227-233.

[6] Hu, Y., Zheng, X., Wang, D., Zhang, Z., Xie, Y., and Yao, Z., 2015, "Application of laser peen forming to bend fibre metal laminates by high dynamic loading," J. Mater. Process. Technol., 226, pp. 32-39.

[7] Gao, H., Hu, Y., Xuan, Y., Li, J., Yang, Y., Martinez, R. V., Li, C., Luo, J., Qi, M., and Cheng, G. J., 2014, "Large-scale nanoshaping of ultrasmooth 3D crystalline metallic structures," Science, 346(6215), pp. 1352-1356.

[8] Mao, B., Liao, Y., and Li, B., 2019, "Abnormal twin-twin interaction in an Mg-3Al-1Zn magnesium alloy processed by laser shock peening," Scripta Mater., 165, pp. 89-93.

[9] Hauer, M., Funk, D., Lippert, T., and Wokaun, A., 2004, "Time resolved study of the laser ablation induced shockwave," Thin Solid Films, 453, pp. 584-588.

[10] Siddaiah, A., Mao, B., Liao, Y., and Menezes, P. L., 2018, "Surface characterization and tribological performance of laser shock peened steel surfaces," Surf. Coat. Technol., 351, pp. 188-197.

[11] Liao, Y., Suslov, S., Ye, C., and Cheng, G. J., 2012, "The mechanisms of thermal engineered laser shock peening for enhanced fatigue performance," Acta Mater., 60(13), pp. 4997-5009.

[12] Zhang, R., Zhou, X., Gao, H., Mankoci, S., Liu, Y., Sang, X., Qin, H., Hou, X., Ren, Z., and Doll, G. L., 2018, "The effects of laser shock peening on the mechanical properties and biomedical behavior of AZ31B magnesium alloy," Surf. Coat. Technol., 339, pp. 48-56.

[13] Ge, M. Z., Xiang, J. Y., Yang, L., and Wang, J. T., 2017, "Effect of laser shock peening on the stress corrosion cracking of AZ31B magnesium alloy in a simulated body fluid," Surf Coat Tech, 310, pp. 157-165.

[14] Lim, H., Kim, P., Jeong, H., and Jeong, S., 2012, "Enhancement of abrasion and corrosion resistance of duplex stainless steel by laser shock peening," J Mater Process Tech, 212(6), pp. 1347-1354.
[15] Rubio-Gonzalez, C., Gomez-Rosas, G., Ruiz, R., Nait, M., and Amrouche, A., 2015, "Effect of laser shock peening and cold expansion on fatigue performance of open hole samples," Struct Eng Mech, 53(5), pp. 867-880.
[16] Shen, N. G., Pence, C. N., Bowers, R., Yu, Y., Ding, H. T., Stanford, C. M., and Ozbolat, I. T., 2014, "Surface Micro-scale Patterning for Biomedical Implant Material of Pure Titanium via High Energy Pulse Laser Peening," Proceedings of the Asme 9th International Manufacturing Science and Engineering Conference, 2014, Vol 2.
[17] Wei, X. L., and Ling, X., 2014, "Numerical modeling of residual stress induced by laser shock processing," Appl Surf Sci, 301, pp. 557-563.
[18] Fabbro, R., Fournier, J., Ballard, P., Devaux, D., and Virmont, J., 1990, "Physical Study of Laser-Produced Plasma in Confined Geometry," J Appl Phys, 68(2), pp. 775-784.
[19] Zhang, W. W., Yao, Y. L., and Noyan, I. C., 2004, "Microscale laser shock peening of thin films, part 1: Experiment, modeling and simulation," J Manuf Sci E-T Asme, 126(1), pp. 10-17.
[20] Berthe, L., Fabbro, R., Peyre, P., Tollier, L., and Bartnicki, E., 1997, "Shock waves from a water-confined laser-generated plasma," J Appl Phys, 82(6), pp. 2826-2832.
[21] Peyre, P., Fabbro, R., Berthe, L., and Dubouchet, C., 1996, "Laser shock processing of materials, physical processes involved and examples of applications," J Laser Appl, 8(3), pp. 135-141.
[22] Peyre, P., Sollier, A., Chaieb, I., Berthe, L., Bartnicki, E., Braham, C., and Fabbro, R., 2003, "FEM simulation of residual stresses induced by laser Peening," Eur Phys J-Appl Phys, 23(2), pp. 83-88.
[23] Wu, B., and Shin, Y. C., 2005, "A self-closed thermal model for laser shock peening under the water confinement regime configuration and comparisons to experiments," J Appl Phys, 97(11).
[24] Wu, B. X., and Shin, Y. C., 2006, "Laser pulse transmission through the water breakdown plasma in laser shock peening," Appl Phys Lett, 88(4).
[25] Wu, B. X., and Shin, Y. C., 2007, "Two dimensional hydrodynamic simulation of high pressures induced by high power nanosecond laser-matter interactions under water," J Appl Phys, 101(10).
[26] Wu, B. X., and Shin, Y. C., 2007, "A one-dimensional hydrodynamic model for pressures induced near the coating-water interface during laser shock peening," J Appl Phys, 101(2).
[27] Wu, B. X., and Shin, Y. C., 2007, "From incident laser pulse to residual stress: A complete and self-closed model for laser shock peening," J Manuf Sci E-T Asme, 129(1), pp. 117-125.
[28] Bellan, P. M., 2006, "Fundamentals of plasma physics," Cambridge University Press.
[29] J.J. MacFarlane, G. A. M., R. R. Peterson, 1995, "BUCKY-1-A 1-D Radiation Hydrodynamics Code for Simulating Inertial Confinement Fusion High Energy Density Plasmas," Wisconsin Fusion Technology Institute.
[30] Stafe, M., Negutu, C., Puscas, N. N., and Popescu, I. M., 2010, "Pulsed Laser Ablation of Solids," Rom Rep Phys, 62(4), pp. 758-770.
[31] Chen, F. F., 1984, Introduction to plasma physics and controlled fusion, Plenum Press, New York.
[32] Duderstadt, J. J., and Moses, G. A., 1982, Inertial confinement fusion, Wiley, New York.
[33] Huda, J. D., 2016, "NRL Plasma Formulary."
[34] Callen, J. D., "Fundamentals of plasma physics."
[35] MacFarlane, J. J., Golovkin, I. E., and Woodruff, P. R., 2006, "HELIOS-CR - A 1-D radiation-magnetohydrodynamics code with inline atomic kinetics modeling," J Quant Spectrosc Ra, 99(1-3), pp. 381-397.
[36] Phelps, A., 1987, "Fundamentals of Plasma Physics - Bittencourt,Ja," Nature, 326(6109), pp. 209-209.
[37] Devaux, D., Fabbro, R., Tollier, L., and Bartnicki, E., 1993, "Generation of Shock-Waves by Laser-Induced Plasma in Confined Geometry," J Appl Phys, 74(4), pp. 2268-2273.
[38] Harilal, S. S., Tillack, M. S., O'Shay, B., Bindhu, C. V., and Najmabadi, F., 2004, "Confinement and dynamics of laser-produced plasma expanding across a transverse magnetic field," Phys Rev E, 69(2).
[39] Harilal, S. S., Miloshevsky, G. V., Diwakar, P. K., LaHaye, N. L., and Hassanein, A., 2012, "Experimental and computational study of complex shockwave dynamics in laser ablation plumes in argon atmosphere," Phys Plasmas, 19(8).